



Journal Name

COMMUNICATION

## Surface-related properties of perovskite $\text{CH}_3\text{NH}_3\text{PbI}_3$ thin films by aerosol-assisted chemical vapour deposition

M. Afzaal,<sup>a\*</sup> B. Salhi,<sup>b</sup> A. Al-Ahmed,<sup>b</sup> H. M. Yates,<sup>a</sup> and A. S. Hakeem<sup>c</sup>Received 00th January 20xx,  
Accepted 00th January 20xx

DOI: 10.1039/x0xx00000x

www.rsc.org/

**A modified three-step aerosol-assisted chemical vapour deposition process was used to grow dense and uniform  $\text{CH}_3\text{NH}_3\text{PbI}_3$  thin films directly on borosilicate glass. The resulting photoluminescence spectrum blue shifted with respect to its bandgap. X-ray photoelectron spectroscopy studies confirmed non-stoichiometric lead:iodine ratios within the films, due to decomposition of  $\text{CH}_3\text{NH}_3\text{PbI}_3$  layers over time into lead iodide and release of ammonia and hydrogen iodide. Complex refractive index and dielectric function of deposited thin films were determined by variable angle spectroscopic ellipsometry.**

Record hybrid perovskite (PK) solar cell efficiencies beyond 22% is a result of high absorption coefficients, large carrier diffusion lengths and high carrier mobility of PK absorber layers.<sup>1-4</sup> Organic-inorganic PK materials are commonly represented with the general formula  $\text{ABX}_3$ , where A is an organic cation, B is a divalent cation and X is a monovalent halide anion. One of the commonly studied perovskite solar cell material, methylammonium lead triiodide ( $\text{CH}_3\text{NH}_3\text{PbI}_3$ ) has a sharp absorption edge<sup>5</sup> with a bandgap ( $E_g$ ) between 1.50 and 1.61 eV<sup>6</sup> and a low difference between open circuit voltage and its bandgap potential,  $E_g/q$ .<sup>5,7,8</sup>

The majority of work reported to-date for improving power conversion efficiencies has focused on spin coating of PK absorber layers on substrates. Issues concerning the scalability and large area deposition of coatings by this processing method remain outstanding. On the contrary, chemical vapour deposition (CVD) processes, which are routinely used in glass-float industry, allow large volume and faster growth rates of films. Many modifications of CVD technique such as hybrid,<sup>9</sup> low-pressure (LP)<sup>10</sup> and atmospheric-pressure (AP)<sup>11</sup> have been

exploited for the deposition of PK thin films. For large-scale deposition of thin films, use of expensive vacuum equipment in LP-CVD limits its potential. Issues about the thermal stability of the organic component of the PK have also been highlighted. Solution based aerosol-assisted (AA) CVD process using aerosol droplets to transport precursors provides an attractive alternative for depositing PK films at atmospheric pressure. Indeed, various groups including ours have demonstrated one-step AACVD method for depositing  $\text{CH}_3\text{NH}_3\text{PbX}_3$  (X = Cl, Br) thin films.<sup>12-14</sup> However, the deposited films tended to be of low density and composed of powdery agglomerates, probably due to early gas phase nucleation between  $\text{PbX}_2$  and  $\text{CH}_3\text{NH}_3\text{X}$  (X = Cl, Br) at deposited temperatures.

Although AACVD is a low-cost and scalable technique, the ability to deposit dense and uniform PK films is challenging. Before the method can be truly regarded for PK-based photonic technologies such as lasers, solar cells or light emitting diodes,<sup>5</sup> it is critical to enable deposition of smooth layers. Any ambiguity in the refractive index (RI) caused by voids or increased surface roughness will result in poor light confinement and inefficient light absorption or reflection in optical thin film devices.<sup>16</sup> In general, information on complex optical properties of CVD deposited  $\text{CH}_3\text{NH}_3\text{PbI}_3$  films is lacking, owing to poor film qualities. Herein, we resort to a three-step AACVD process originally proposed by Chen<sup>15</sup> with significant changes to deposit PK thin films of ca. 400 nm in thickness. **This value has been shown to maximise the short circuit current, while keeping the film smooth.**<sup>1</sup> For producing uniform films with target thickness, modifications included a constant nitrogen ( $\text{N}_2$ ) flow rate of 0.6 l/min throughout the experiment, adjusting precursor ratio, a set deposition time of 1 hr and the use of dimethylformamide (DMF) as oppose to methanol (MeOH) for the intercalation, as MeOH due to its higher vapour pressure, resulted in partial transfer of  $\text{CH}_3\text{NH}_3\text{I}$  into the reaction chamber. Full details are appended in the supplementary experimental section. In this paper we accurately determined the optical constants and absorption coefficients for the first time for CVD deposited PK films *via* use

<sup>a</sup> Materials and Physics Research Centre, The University of Salford, Salford, M5 4WT, United Kingdom. E-mail: M.Afzaal@salford.ac.uk

<sup>b</sup> Center of Research Excellence in Renewable Energy, King Fahd University of Petroleum & Minerals, Dhahran, 31261, Saudi Arabia

<sup>c</sup> Center of Research Excellence in Nanotechnology, King Fahd University of Petroleum & Minerals, Dhahran, 31261, Saudi Arabia

Electronic Supplementary Information (ESI) available: Experimental work, characterisation techniques, transmission and reflection spectra

of variable angle spectroscopic ellipsometry (VASE) to yield important complex dielectric function and refractive index over the full spectral range.

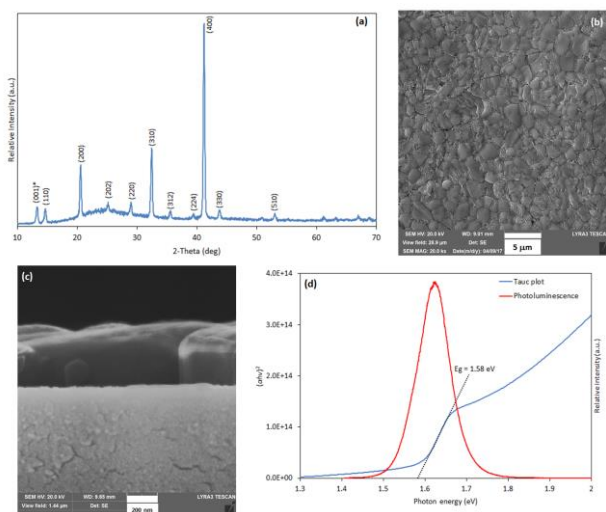


**Fig. 1** (a) X-ray powder diffraction, (b) top-surface and (c) cross-section scanning electron microscope images. (d) blue curve: Tauc plot, red curve: photoluminescence spectrum of deposited  $\text{CH}_3\text{NH}_3\text{PbI}_3$  films.

Use of a modified three step cold-wall AACVD process shown in Figure S1 yielded uniform and adhered  $\text{CH}_3\text{NH}_3\text{PbI}_3$  films, although these could be scratched by a scalpel. This is in contrast to one-step process where the film surface could be easily wiped with a tissue.<sup>13,14</sup> To replicate film thicknesses between 300-400 nm often required for the fabrication of efficient PK solar cells, substantial changes were made to the original recipe as mentioned earlier.<sup>15</sup>

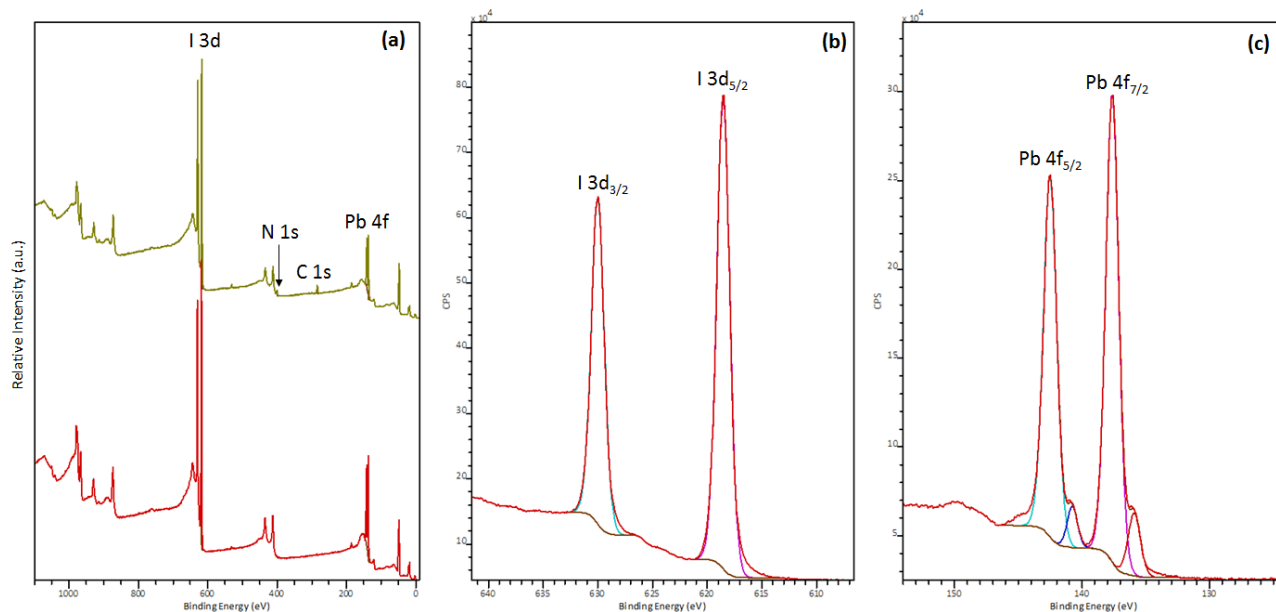
The X-ray powder diffraction pattern shows the formation of room temperature stable tetragonal  $\text{CH}_3\text{NH}_3\text{PbI}_3$  structure, with a minor impurity at  $12.9^\circ$  corresponding to  $\text{PbI}_2$  (Figure 1a,

Table S1). According to Scherrer's equation, the particle size was estimated to be  $\sim 30$  nm. The corresponding surface scanning electron microscope (SEM) image confirms the deposition of dense, uniform and pinhole free films, with an average thickness of  $393 \pm 26$  nm estimated using a cross-section SEM image (Figure 1b and c). The film thickness was measured at different points along the film, so the standard deviation given here is a measure of the thickness variation. As described earlier the smoothness of the film is a critical factor.

The optical transmission and reflection spectra given in Figure S2 shows a steep drop at around 800 nm with an absorption edge at  $\sim 1.55$  eV and is similar to that seen in previous work.<sup>8</sup> The  $E_g$  was determined from a direct bandgap Tauc plot of  $(\alpha h\nu)^2$  versus energy in eV where  $\alpha$  is the absorption coefficient (derived from  $\alpha = -\ln[T/(1-R)]/t$  where  $T$ =transmission,  $R$ =reflection and  $t$ =film thickness) and  $h\nu$  is the photon energy. Extrapolating the linear region to the energy-axis intercept yields  $E_g$  with 1.58 eV (Figure 1d). The photoluminescence spectrum shows an emission peak at 1.63 eV with full width at half maximum of 44 meV, which is blue shifted in energy relative to its  $E_g$ . One possible reason postulated behind this shift is the presence of trap states below its band edge.<sup>17</sup> Another contributing factor to this downshift could be due to a polaronic effect.<sup>18</sup>

X-ray photoelectron spectroscopy was used to probe the surface chemistry of deposited PK films. In spite of previous attempts, surface chemistry of  $\text{CH}_3\text{NH}_3\text{PbI}_3$  remains less well understood.<sup>13,15</sup> The survey scan established the presence of Pb, I, N and C and showed only impurities of a very small O 1s and a C 1s related to amorphous C (Figure 2a). These were removed by a 10 sec Ar etch, confirming that they related to environmental surface contaminants. In contrast the intensity of the Pb and I related peaks increased (Figure 3a).

The high resolution I 3d scan shows the major  $3d_{5/2}$  peak at 618.5 eV and the  $3d_{3/2}$  at 630.0 eV (Figure 2b). The splitting of



**Fig. 2** (a) Wide scan X-ray photoelectron spectra of non-etched (top) and etched (bottom)  $\text{CH}_3\text{NH}_3\text{PbI}_3$  sample. High resolution XPS scans of etched (b) I 3d and (c) Pb 4f.

these ( $\Delta = 11.5$  eV) and a branching ratio of 1.5, along with their position establishes the presence of a single I component in the film.<sup>19</sup> The Pb 4f shows the presence of two distinct Pb species (Figure 2c). The major signal is a doublet with the 4f<sub>7/2</sub> at 137.6 eV and 4f<sub>5/2</sub> at 142.5 eV in agreement with Pb within PK. There is also a lower intensity signal with 4f<sub>7/2</sub> at 135.9 eV related to metallic Pb.<sup>20</sup> This was approximately 10% of the total lead content. The presence of metallic Pb has previously been seen by other researchers and has been ascribed to decomposition during annealing,<sup>21</sup> laser irradiation<sup>22</sup> or beam damage during measurements.<sup>23</sup>

N 1s at 401.5 eV is in line with that reported by Zou et al.<sup>24</sup> and assigned to the N within the methylammonium ion. Although, this is of much lower intensity than would be expected and partially submerged in the Pb 4d<sub>3/2</sub> signal. This suggests that there has been some decomposition of the PK. Exposure of films to air and moisture has been shown to lead to the decomposition of the PK to PbI<sub>2</sub> and the release of the NH<sub>3</sub> and HI into the air.<sup>25</sup> This would lead to the loss of the N 1s signal and a reduction of the I signal in relation to the Pb. As there was a delay between deposition and analysis during which the samples were at times exposed to air so it is very likely some decomposition took place, although to eye still looked black and no obvious signs of yellow PbI<sub>2</sub>. In addition, there is no sign of any O 1s signals suggesting that there has been no high level absorption of moisture, unlike that seen by Wang.<sup>25</sup> The presence of some Pb metal as described above also supports the possible part decomposition, although this could still be in part due to XPS beam damage.

The metallic Pb was removed from the basic components when calculating the stoichiometry. For non-etched samples this led to a Pb:I:N ratio of 1:2.5:0.5. For the non-etched samples the level of surface C impurities was too high to estimate the C related to PK. This would suggest the surface consisted of mainly PbI<sub>2</sub> with some remaining PK. Etched samples produced ratios of Pb:I:N:C ratio of 1:2:0.1:0.1. The values obtained for N and C in XPS are not accurate due to the low intensity of the peak and poor signal/noise level. Once etched with contaminants removed this confirmed the majority species on the surface was PbI<sub>2</sub>. XPS is a very surface sensitive technique only sampling the top few nm's of a material so this result confirms the film surface had decomposed due to beam damage during measurement and delay in measurement (last data obtained). That it is only the surface can be confirmed as no yellow PbI<sub>2</sub> could be seen, only the black colouration of the PK. This is confirmed by energy dispersive X-ray spectroscopy (Figure S3) which will penetrate into the bulk of the film. This gave Pb:I ratios ranging between 1:2.6 and 1:2.8, in line with the presence of PK. Transmission data, which will penetrate the entire film re-enforced this result.

Spectroscopic ellipsometry was used to determine the optical properties by fitting a multi-oscillator model to the  $\psi$  and  $\Delta$  measurements taken at 60°, 70° and 75°. Figure 3a shows a good agreement (MSE = 7.16) between the experimental data of  $\psi$  and  $\Delta$ , and the fitting results across the full spectral range. From the spectra, we observe two peaks above their absorption edge ( $> 1.61$  eV) located at around 2.63 and 3.72 eV. These

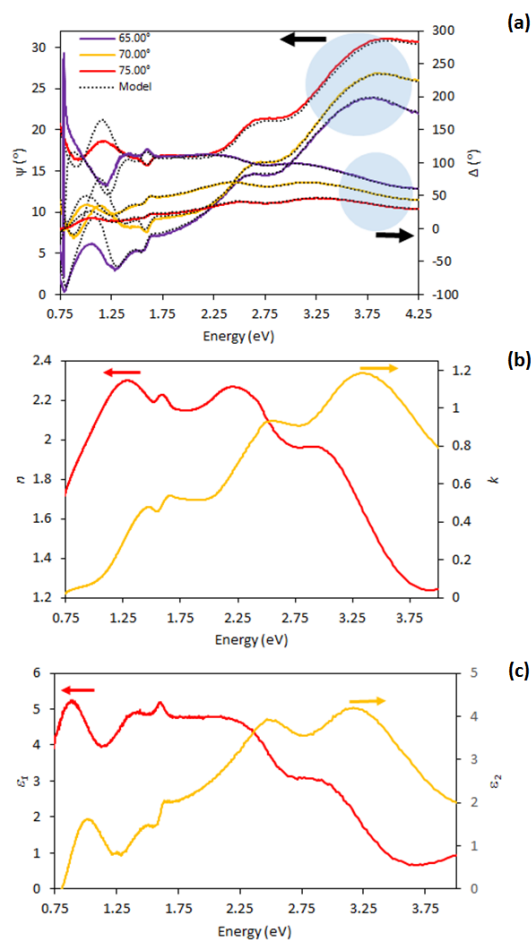


**Fig. 3** Variable angle spectroscopic ellipsometry data and fits to  $\psi$  and  $\Delta$  of CH<sub>3</sub>NH<sub>3</sub>PbI<sub>3</sub> film at three different angles of incidence; 65°, 70° and 75°. (b) Refractive index ( $n$ ,  $k$ ) and (c) dielectric function ( $\epsilon_1$ ,  $\epsilon_2$ ) of CH<sub>3</sub>NH<sub>3</sub>PbI<sub>3</sub>.

values are in close proximity to those found by Löper et al.<sup>8</sup> The modelled film thickness 0.417  $\mu\text{m}$  ( $\pm 0.64$  nm) treated as a free parameter is in-line with the value determined from SEM image as mentioned above (0.393  $\mu\text{m}$ ).

Turning to the complex refractive index ( $N = n - ik$ , where  $n$  is the refractive index and  $k$  is the extinction coefficient). Figure 3b shows the refractive index spectra ( $n$ ,  $k$ ) of the bulk of the material against wavelength. For  $k(\lambda)$  we observe three oscillations, one located at 1.66 eV or 747 nm, the second at 2.50 eV or 491 nm and third at 3.34 eV or 367 nm. As clearly shown by Leguy et al. all three absorption peaks corresponds to transitions between highest valence band and the lowest conduction band at points in the pseudocubic Brillouin zone.<sup>26</sup> The absorption peak at 747 nm is a result of transition from the first valence band maximum to lowest conduction band at the  $R$  symmetry point in the first Brillouin zone.<sup>27</sup> The second peak at 491 nm is a result of transition from the lower valence band to the conduction band minimum at the  $M$  point. As for the third peak at 367 nm, it is assigned to electron transfer from highest valence band to lowest conduction band at the  $X$  point.<sup>26</sup> As expected, the observed  $n(\lambda)$  values are lower than that of corresponding single crystals, primarily due to the presence of surface imperfections and/or different material

densities, which are effected by deposition methods and their associated parameters.<sup>16</sup> Nevertheless, with  $n \approx 2.3$  in the visible region and its matching-index with silicon (Si),<sup>28</sup> it can have important implications as an antireflective coating for tandem cells. The relative high  $k$  value in comparison with for example, cadmium telluride and Si gives  $\alpha \gtrsim 10^5 \text{ cm}^{-1}$  for the full spectral range as shown below and confirming its light absorbing property in very thin form. From the dielectric functions of  $\text{CH}_3\text{NH}_3\text{PbI}_3$  given in Figure 3c, we obtained 5.1 for the  $\epsilon_1$  ( $\epsilon_1 = n_2 - k_2$ ) near the absorption edge (1.6 eV) and is very similar to that reported by Shirayama et al.<sup>29</sup> The measurement was made in air, which allows us to attribute the peak observed at 3.20 eV to the formation of the hydrated phase on the surface.<sup>30</sup> For  $\epsilon_2$  ( $\epsilon_2 = 2nk$ ), the absorption edge of around 1.6 eV is consistent with the previous work<sup>8</sup>, albeit of slightly low value.

Independent measures of  $E_g$  via ellipsometry and spectrophotometry were compared to validate the values obtained. Figure 4 shows plots of  $\alpha$  derived from the  $n$  using  $4\pi k/\lambda$  ( $\lambda$  is free space wavelength) and using  $T$  and  $R$  measurements, as mentioned above. Both spectra in terms of shape and amplitude correspond well with each other over the range of interest. For  $\alpha$  calculated using  $n$  (via ellipsometry), we can see three distinct peaks, one at 1.6 eV attributed to the bandgap and the other two at  $E = 2.5$  eV and  $E = 3.5$  eV can be explained by the absorption according to earlier work.<sup>27,29</sup> In the same spectrum, we can observe low absorption at  $E_g$  which is attributed to the non-excitonic optical transition. The broad peak observed at 2.5 eV and 3.5 eV can be attributed to optical transition in  $\text{CH}_3\text{NH}_3\text{PbI}_3$  due to the nonexcitonic interband transition within the  $\text{PbI}_3^-$ . Note that the optical characteristics are influenced by the surface roughness of the  $\text{CH}_3\text{NH}_3\text{PbI}_3$  and existence of hydrate phase close to the surface region<sup>29</sup> and to the fact the film is composed of  $\text{CH}_3\text{NH}_3\text{PbI}_3$  layers.

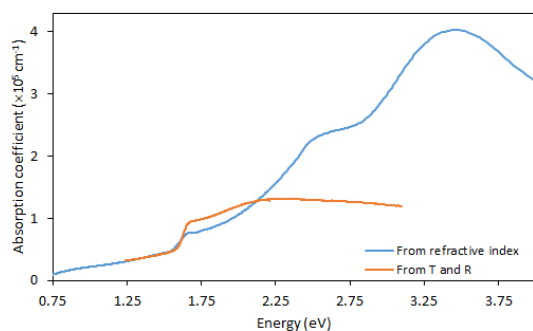


**Fig. 4** A comparison of absorption coefficients calculated. T and R refer to transmission and reflection, respectively.

In summary, three-step aerosol-assisted chemical vapour deposition process has been demonstrated to grow high quality  $\text{CH}_3\text{NH}_3\text{PbI}_3$  thin films with strong absorption and emission characteristics. Although the bulk of the film is  $\text{CH}_3\text{NH}_3\text{PbI}_3$ , the surface chemistry of deposited films showed transformation of perovskite layers into  $\text{PbI}_2$ ,  $\text{NH}_3$ , HI and the loss of nitrogen which accounts for the deviation from ideal  $\text{Pb:I} = 1:3$  stoichiometry within the films. For the first time, variable angle

spectroscopic ellipsometry has been used to determine the refractive index, dielectric functions and absorption coefficient properties of CVD deposited  $\text{CH}_3\text{NH}_3\text{PbI}_3$  thin films.

This work was financed by EU Horizon 2020 grant H2020-LCE-2015-16-53296 CHEOPS. We thank Dr J. E. Proctor and H. Malik (University of Salford) for their help with the PL measurements.

## Notes and references

- M. A. Green, A. Ho-Baillie and H. J. Snaith, *Nat. Photonics*, 2014, **8**, 506.
- P. Gao, M. Gratzel, and M. K. Nazeeruddin, *Energy Environ. Sci.* 2014, **7**, 2448.
- S. D. Stranks, H. J. Snaith, *Nat. Nanotechnol.* 2015, **10**, 391.
- M. Petrović, V. Chellappan and S. Ramakrishna, *Sol. Energy*, 2015, **122**, 678.
- S. De Wolf, J. Holovsky, S.-J. Moon, P. Löper, B. Niesen, M. Ledinsky, F.-J. Haug, J.-H. Yum and C. Ballif, *J. Phys. Chem. Lett.*, 2014, **5**, 1035.
- S. A. Bretschneider, J. Weickert, J. A. Dorman, L. Schmidt-Mende, *APL Mater.*, 2014, **2**, 040701-1.
- H. J. Snaith, *J. Phys. Chem. Lett.*, 2013, **4**, 3623.
- P. Löper, M. Stuckelberger, B. Niesen, J. Werner, M. Filipic, S. J. Moon, J.-H. Yum, M. Topic, S. De Wolf and C. Ballif, *J. Phys. Chem. Lett.*, 2015, **6**, 66.
- M.R. Leyden, L.K. Ono, S.R. Raga, Y. Kato, S. Wang and Y. Qi, *J. Mater. Chem. A* 2014, **2**, 18742.
- P. Luo, Z. Liu, W. Xia, C. Yuan, J. Cheng and Y. Lu, *ACS Appl. Mater. Interfaces*, 2015, **7**, 2708.
- Q. Chen, H. Zhou, Z. Hong, S. Luo, H.-S. Duan, H.-H. Wang, Y. Liu, G. Li and Y. Yang, *J. Am. Chem. Soc.*, 2013, **136**, 622.
- D. J. Lewis and P. O'Brien, *Chem. Commun.*, 2014, **50**, 6319.
- D. S. Bhachu, D. O. Scanlon, E. J. Saban, H. Bronstein, I. P. Parkin, C. J. Carmalt and R. G. Palgrave, *J. Mater. Chem. A* 2015, **3**, 9071.
- M. Afzaal, and H. M. Yates, *Surf. Coat. Tech.*, 2017, **321**, 336.
- S. Chen, *Thin Films Deposition for Energy Efficient Windows and Solar Cells*, PhD Thesis, Queen Mary University of London, London. 2016.
- M. S. Alias, I. Dursun, M. I. Saidaminov, E. M. Diallo, P. Mishra, T. K. Ng, O. M. Bakr and B. S. Ooi, *Opt Express*, 2016, **24**, 16586.
- R. L. Milot, G. E. Eperon, H. J. Snaith, M. B. Johnston, L. M. Herz, *Adv. Funct. Mater.*, 2015, **25**, 6218.
- M. Pope, C. E. Swenberg, *Electronic Processes in Organic Crystals and Polymers*; Oxford Science: New York, 1999
- R. Lindblad, D. Bi, B.-W. Park, J. Oscarsson, M. Gorgoi, H. Siegbahn, M. Odelius, E. M. J. Johansson, and H. Rensmo, *J. Phys. Chem. Lett.*, 2015, **5**, 648.
- J. Chastain and J. F. Moulder. *Handbook of XPS*; Perkin-Elmer Corporation: Eden Prairie, MN, 1995.
- H. Xie, X. Liu, L. Lyu, D. Niu, Q. Wang, J. Huang and Y. Gao, *J. Phys. Chem. C* 2016, **120**, 215.
- Y. Li, X. Xu, C. Wang, B. Ecker, J. Yang, J. Huang and Y. Gao, *J. Phys. Chem. C* 2017, **121**, 3904.
- S. R. Raga, M.-C. Jung, M. V. Lee, M. R. Leyden, Y. Kato, and Y. Qi, *Chem. Mater.*, 2015, **27**, 1597.
- Y. Zou, Q. Meng, H. Mao and D. Zhu, *Org. Electronics*, 2017, **41**, 307.
- C. Wanga, Y. Li, X. Xu, C. Wang, F. Xie and Y. Gao, *Chem. Phys. Lett.* 2016, **649**, 151.
- A. M. A. Leguy, P. Azarhoosh, M. I. Alonso, M. Campoy-Quiles, O. J. Weber, J. Yao, D. Bryant, M. T. Weller, J. Nelson, A. Walsh, M. van Schilfgaarde, P. R. F. Barnes and P. R. F. Barnes, *Nanoscale*, 2016, **8**, 6317.

- 27 G. Xing, N. Mathews, S. Sun, S. S. Lim, Y. M. Lam, M. Grätzel, S. Mhaisalkar and T. C. Sum, *Science*, 2013, **432**, 344.
- 28 L. J. Phillips, A. M. Rashed, R. E. Treharne, J. Kay, P. Yates, I. Z. Mitrovic, A. Weerakkody, S. Hall and K. Durose, *Sol. Energy Mater. Sol. Cells*, 2016, **147**, 327.
- 29 M. Shirayama, H. Kadowaki, T. Miyadera, T. Sugita, M. Tamakoshi, M. Kato, T. Fujiseki, D. Murata, S. Hara, T. N. Murakami, S. Fujimoto, M. Chikamatsu and H. Fujiwara, *Phys. Rev. Appl.*, 2016, **5**, 14012.
- 30 M. Hirasawa, T. Ishihara and T. Goto, *J. Phys. Soc. Japan*, 1994, **63**, 3870.